Available online at www.sciencedirect.com
ScienceDirect
Journal of Power Sources 178 (2008) 269–281
JOURNAL OF POWER SOURCES
www.elsevier.com/locate/jpowsour

Three-dimensional, single-phase, non-isothermal CFD model of a PEM fuel cell☆

Carlos Martínez Baca [a,*], Rowland Travis [a], Mads Bang [b]

[a] *Department of Mechanical Engineering, Imperial College, London Exhibition Road, South Kensington, London SW7 2AZ, UK*
[b] *Institute of Energy and Technology, Aalborg University, Aalborg, Denmark*

Received 29 August 2007; received in revised form 14 November 2007; accepted 1 December 2007

Abstract

A comprehensive, three-dimensional analysis of a polymer electrolyte membrane (PEM) fuel cell has been developed to study the performance of this device under different operational conditions. This steady-state analysis is single-phase and non-isothermal. A commercial computational fluid dynamics (CFD) program provided a numerical platform for solving the conservation equations for species, energy, charge, mass and momentum. Different boundary conditions were added to a computational domain to simulate single channel PEM fuel cell. The electrochemistry involved in this model was added by a set of user-defined subroutines that feature: electrochemical reactions, electric and ionic charge and heat generation. The calculations were then solved by an iterative method following an adapted computational procedure. The results were validated with other computational models and experimental data. These show a noticeable non-uniform distribution of the current density across the catalyst layer (CL) at different operational conditions. The results emphasize on the differences of anodic and cathodic activation overpotentials, the oxygen transport limitations and the ohmic losses distributions of both proton and electric overpotentials.

Keywords: Computational fluid dynamics; Single-phase; Non-isothermal; Electroosmotic; Overpotentials

1. Introduction

A fuel cell is as an electrochemical converter. It can be said that a fuel cell is a device that converts chemical energy into electrical power and ideally can continue to operate as long as it is fed with suitable fuels and oxidants and the reaction products are being removed.

Electrochemical power sources differ from others, such as thermal power plants because the energy conversion occurs without any intermediate steps. For example, in the case of thermal power plants, fuel is first converted into thermal energy and then into electric power via generators. In fuel cells systems this multi-step process is achieved by electrochemical reactions. As a consequence, electrochemical systems show some advantages, such as energy efficiency.

There is extensive literature available on numerical ways of modelling fuel cells. Polymer electrolyte membrane (PEM) fuel cells have been modelled for more than 15 years. Although one-dimensional in nature some of the early analyses remain the basis for most of the more elaborated models to date. Bernardi and Verbrugge [5] made a big emphasis on the electrochemistry and diffusive processes inside the fuel cell's membrane electrode assembly (MEA). Springer et al. [22] provided a great insight into the water transport process inside the MEA. Ticianelli et al. [25] made a numerical model which introduced a way of calculating locally the cell potential. Fuller and Newman [11] produced a model that could predict the performance of the cell along a longitudinal channel by integrating the solution at various points down the channel. They pinpointed the effect of dehydration in the fuel cell's membrane due to the electroosmotic drag. Lampimen and Fomino [15] introduced entropy changes in to their model. Gurau et al. [12] used a special handling of the transport equations which enabled them to use the same numerical method for a unified computational domain. This domain constituted a polymer membrane, two catalyst layers (CLs), two gas diffusers (GDs) and two feeding channels.

☆ The work presented in this paper is part of C. Martínez Baca's PhD at Imperial College.

* Corresponding author. Tel.: +44 7990615222.
E-mail address: carlos.martinez@rrfcs.com (C.M. Baca).

0378-7753/$ – see front matter © 2007 Elsevier B.V. All rights reserved.
doi:10.1016/j.jpowsour.2007.12.023

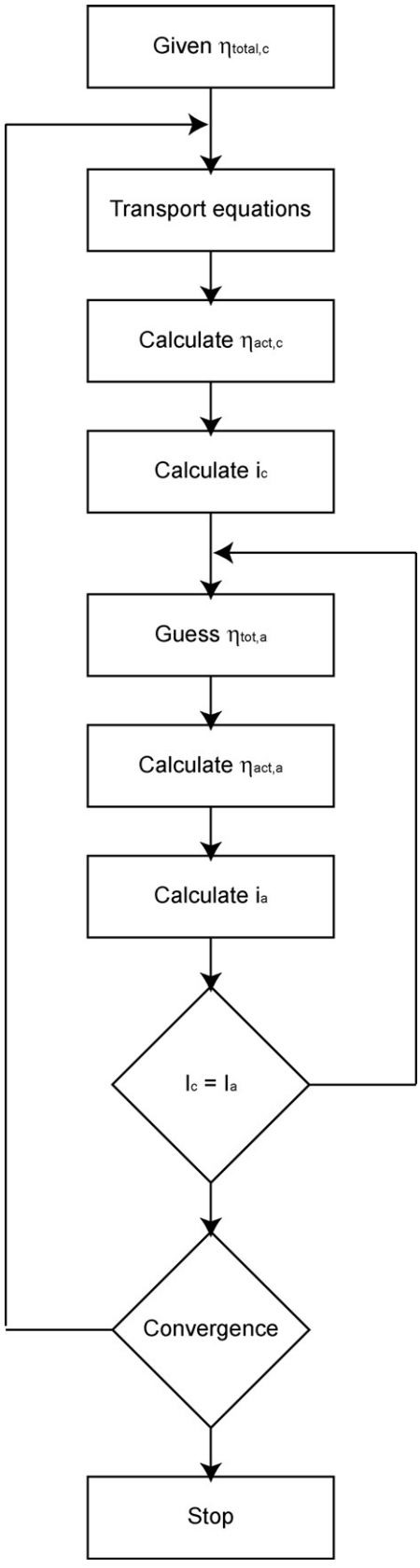

Fig. 1. Diagram of the solution procedure.

This in turn eliminated the need for prescribing arbitrary boundary conditions for the fuel cell interfaces. The papers mentioned above are the foundation of the model presented in this paper.

As PEM fuel cell models were becoming more specific, people began to realize that one of the most complicated issues in their analyses was the transport of water in the PEM. Zawodzinski et al. [28] experimented on several types of proton exchange membranes. They reported water sorption characteristics, diffusion coefficient, electroosmotic drag and conductivity. Van Zee et al. [16] and Shimpalee et al. [17] conducted a thorough experiment concerning water transport in the membrane that was validated with a numerical model. Most of their papers conclude that the velocity of the water inside the membrane is too small and has little effect on the overall water mass flow rate. Later on Zawodzinski et al. [27] and more recently Kulikovsky [14] and Sui and Djilali [23] confirmed that the electroosmotic drag coefficient can be considered as constant for a wide range of water content in the membrane.

The three-dimensional PEM fuel cell model, presented by Dutta et al. [9] showed how to modify a commercial computational fluid dynamics (CFD) code to include the necessary electrochemical processes. This and subsequent publications [10,18] stressed the importance of the diffusive and convective transport of reactants and products in the MEA and feeding channels. These publications also introduced geometric changes in their analyses. This approach derived in a better understanding of the overall geometry of the cell and gave way to numerous design analyses. Later, some papers focused exclusively on how to optimise the dimensions of specific PEM fuel cell components such as gas channel aspect ratios, gas diffusers and electrolyte thicknesses, nafion content on CLs and catalyst porosities (Fig. 1).

Most PEM fuel cell models available in the literature assume that the electrochemical reactions take place at an interface between the diffusers and the electrolyte. It is convenient to model CLs as interfaces because it is possible to define arbitrary boundary conditions at both surfaces of this "wall" such as heat transfer, mass sources or fixed temperature and concentrations. In reality CLs are normally a few microns thick and in this paper we address the distributions of the activation overpotentials and current densities across the CLs. The computational procedure presented in this model is able to measure spatial distribution of these losses inside these thin layers. In general we try to predict the distributions of the overpotentials across the model's MEA.

2. Model description

2.1. Fuel cell principles

The computational domain of our model is shown in Fig. 2. The model constitutes the anode, cathode and electrolyte regions of a PEM fuel cell. Hydrogen-rich fuel is fed in to the anode channel, where part of this travels across the GD. At the anode CL an oxidation reaction splits the hydrogen into protons and electrons according to:

$$H_2 \rightarrow 2H^+ + 2e^- \quad (1)$$

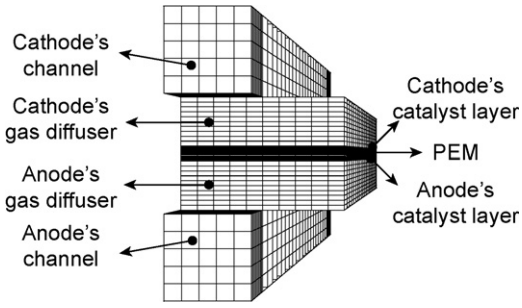

Fig. 2. Computational domain of the model.

Driven by an electric field, the protons migrate across the PEM from the anode towards the cathode. The free electrons are conducted across the cell normally through the platinum supported carbon black particles embedded in the CLs, then through the electric conductive fibers of the GDs, the current collectors (CCs) and through an external circuit which may include a load and back again finishing at the cathode CL (see Scheme 1).

The cathode channels are fed with air. The oxygen in the air travels through the GD towards the CL where it combines with the migrating protons and the electrons to form water according to the following exothermic reduction reaction:

$$\tfrac{1}{2}O_2 + 2H^+ + 2e^- \rightarrow H_2O \quad (2)$$

The overall process, consumes reactants generating electricity, water and heat.

The steady-state PEM fuel cell model presented in this paper is three-dimensional, single-phase and non-isothermal and it comprises the following features:

- multi-component flow,
- convective and conductive heat transfer,
- transport of species across a porous media,
- electrochemical reactions,
- electric and protonic charge conduction.

The equations governing these processes include the full mass, momentum, species, charge and energy conservation equations. Given some appropriate boundary conditions, an extensive suite of user subroutines and a costumed iterative procedure, the commercial CFD solver Star-CD v3.24 provided the numerical platform to process the calculations.

This model assumes that the gases in the channels, GDs and CLs behave as compressible ideal gases and that the membrane is "electroneutral" and behaves as a gas barrier. It is also assumed that there is a constant potential at the interface between the anode GD and the CCs. Further, these interfaces and the channels/CCs interfaces are assumed to be adiabatic. We think that the biggest limitation of this model is the assumption of single-phase modelling.

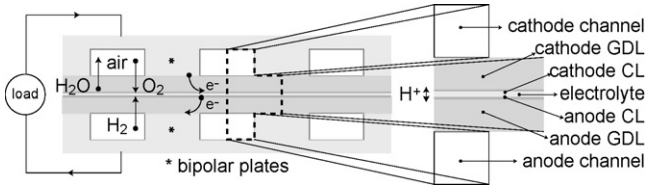

Scheme 1. Schematic PEM fuel cell.

2.2. Model's domain and geometry

Fig. 2 shows the model's computational domain. It contains around 30,000 nodes divided into four separate domains. These are: channels, GDs, CLs and a PEM.

The channels are 12 mm long and have a cross sectional area of 0.25 mm^2. The MEA represents the GDs, CLs and electrolyte. It is 10 mm long, 1 mm wide and 0.69 mm thick. The GD, CL and electrolyte are 300, 20 and 50 μm thick, respectively.

2.3. Electrochemical reaction rate

The local current densities, i_a and i_c, can be accurately predicted at each of the catalyst layers elements according to Bard and Faulkner [3]. The correct implementation of the Butler-Volmer equation in the model gives the local current density at the cathode (Eq. (3)) and anode (Eq. (4)) catalyst layers.

$$i_c = i_{0,c} X_{O_2} \left[\exp\left(\frac{4\alpha_c F}{RT} \eta_{act,c} \right) - \exp\left(-\frac{4(1-\alpha_c)F}{RT} \eta_{act,c} \right) \right] \quad (3)$$

$$i_a = i_{0,a} X_{H_2}^{0.5} \left[\exp\left(\frac{2\alpha_a F}{RT} \eta_{act,a} \right) - \exp\left(-\frac{2(1-\alpha_a)F}{RT} \eta_{act,a} \right) \right] \quad (4)$$

where $i_{0,c/a}$, $\eta_{act,c/a}$ and $\alpha_{a/c}$ are the exchange current densities, the activation overpotentials and the transfer coefficients, respectively. Subscripts a and c refer to anode and cathode, respectively. The two unknown variables in these equations are the concentration of the reactants and the activation overpotentials. The concentration of the reactants is solved by the conservation of species equation in the catalyst layers (see Section 2.4.3). The activation overpotentials have a special solving procedure which is given below in Section 2.5.

2.4. Model equations

This model has been programmed to work with two gas mixtures, hydrated hydrogen and hydrated air. The transport of gas mixtures is solved by the mass (Eq. (5)), momentum (Eq. (6)) and energy (Eq. (11)) conservation equations:

$$\frac{\partial}{\partial x_j}(\rho u_j) = s_p \quad (5)$$

$$\frac{\partial}{\partial x_j}(\rho u_j u_i - \tau_{ij}) = -\frac{\partial P}{\partial x_i} \tag{6}$$

where s_p is the mass source term, x_i are the cartesian coordinates ($i = x, y, z$), u_i the absolute fluid velocity component in direction x_i, τ_{ij} the viscous stress tensor components, P the pressure and ρ the density.

The viscous stress tensor component τ_{ij} in Eq. (6) is calculated as follows:

$$\tau_{ij} = \mu\left(\frac{\partial u_i}{\partial x_j} + \frac{\partial u_j}{\partial x_i}\right) - \frac{2}{3}\mu\frac{\partial u_k}{\partial x_k}\delta_{ij} \tag{7}$$

where μ is the molecular viscosity, δ_{ij} the Kronecker delta.

Each species m of the gas mixtures, whose local concentration is expressed as a mass fraction Y_m, is assumed to be governed by a species conservation equation of the form:

$$\frac{\partial}{\partial x_j}\left(\rho u_j Y_m - D_m\rho\frac{\partial Y_m}{\partial x_j}\right) = s_m \tag{8}$$

where s_m the rate of mass production of species m and D_m is the molecular diffusivity of species m.

The molecular diffusivity of the gas mixtures changes due to temperature, pressure and species concentrations. During operation, fuel cells vary their gas compositions due to chemical reactions. Therefore a variable diffusion coefficient for the gases is needed.

In a binary gas mixture with components m and n, such as hydrogen and water vapour, the binary diffusion coefficients, D_{mn}, can be approximated by Eq. (9) according to Cussler [8]:

$$D_{mn} = D_{mn,\mathrm{ref}}\frac{P_{\mathrm{ref}}}{P}\left(\frac{T}{T_{\mathrm{ref}}}\right)^{1.75} \tag{9}$$

where $D_{mn,\mathrm{ref}}$ is the reference diffusion coefficient of the mixture at pressure P_{ref} and temperature T_{ref}. In ternary systems, the calculation of effective diffusion coefficients can become very complex. Nevertheless PEM fuel cells operate at a range of temperatures and pressures which allow alternative approximation methods to these coefficients to be as accurate as the traditional and more elaborate models. Mills [20] suggested a relation based on a "mixture rule" that proves applicable to PEM fuel cell gas mixtures [2], such as oxygen, nitrogen and water vapour, and is given as

$$D_{m,\mathrm{mix}} = \frac{1 - X_m}{\sum_{n=1;n\neq m}^{N}(X_n/D_{mn})} \tag{10}$$

where X_m refers to the molar fraction of species m. Eq. (10) calculates the effective diffusion coefficient, $D_{m,\mathrm{mix}}$ of species m in a mixture composed of several different components. For further insight into the validation and background of Mills's model please refer to [1].

Heat transfer is implemented with Eq. (11). This is obtained by multiplying the species conservation equation (Eq. (8)) of each species m of the mixture by its heat of formation, H_m, and subtracting it from the energy conservation equation.

$$\frac{\partial}{\partial x_j}\left(\rho h_t u_j - k\frac{\partial T}{\partial x_j} + \sum_m h_{t,m}\rho v_{m,j}\right) = u_j\frac{\partial P}{\partial x_j} + \tau_{ij}\frac{\partial u_i}{\partial x_j} + s_h - \sum_m H_m s_m \tag{11}$$

Here s_m is the rate of production or consumption of species m due to a chemical reaction, k is the thermal conductivity, $v_{m,j}$ the diffusion velocity vector in the j direction and $h_{t,m}$ the thermal enthalpy of species m which is defined by Eq. (11)

$$h_t = \bar{c}_p T - c_{p,\mathrm{ref}}T_{\mathrm{ref}} \tag{12}$$

where $\bar{c}_p$ is the mean constant-pressure specific heat at temperature T and $c_{p,\mathrm{ref}}$ a reference specific heat at temperature T_{ref}.

The reactants and products are assumed to behave as ideal gases, thereby the density ρ of the gas mixture is calculated with

$$\rho = \frac{P}{\bar{R}T(\sum_m (Y_m/M_m))} \tag{13}$$

where M_m is the molecular weight of species m.

2.4.1. Conservation equations in the channels

The transport of gaseous species in the fuel cell channels, is modelled with the following conservation equations for mass (Eq. (14)), momentum (Eq. (15)), species (Eq. (16)) and energy (Eq. (17))

$$\frac{\partial}{\partial x_j}\left(\rho u_j\right) = 0 \tag{14}$$

$$\frac{\partial}{\partial x_j}(\rho u_j u_i - \tau_{ij}) = -\frac{\partial p}{\partial x_i} \tag{15}$$

$$\frac{\partial}{\partial x_j}\left(\rho u_j Y_m - D_{m,\mathrm{mix}}\rho\frac{\partial Y_m}{\partial x_j}\right) = 0 \tag{16}$$

$$\frac{\partial}{\partial x_j}\left(\rho h_t u_j - k_{\mathrm{mix}}\frac{\partial T}{\partial x_j} + \sum_m h_{t,m}\rho v_{m,j}\right) = u_j\frac{\partial P}{\partial x_j} + \tau_{ij}\frac{\partial u_i}{\partial x_j} \tag{17}$$

where k_{mix} is the mixture heat conductivity of species m given by Eq. (18)[19] formula

$$k_{\mathrm{mix}}^{\mathrm{eff}} = \frac{1}{2}\left[\left(\sum_{n=1}^{N}X_n k_n + 1\right)\left(\sum_{n=1}^{N}\frac{X_n}{k_n}\right)^{-1}\right] \tag{18}$$

where k_n is the thermal conductivity of component n.

The velocities at the inlet boundary of the channels were set as a function of the total current produced, I, the channel

cross sectional area, A_{ch} and the stoichiometric ratio ζ. The stoichiometry ratio, ζ, is defined as

$$\zeta = \frac{\text{mass of fuel or oxidant input to the cell}}{\text{mass of fuel or oxidant reacted in the cell}} \tag{19}$$

The total current is a variable dependent on the cell overpotentials and species concentrations that change during the solution procedure. Therefore velocities are updated on an iterative basis, so that the stoichiometric ratios at the inlet boundaries are always kept constant. These are given as

$$u_c = \zeta_c \frac{M_{O_2} I}{Y_{O_2,in}\rho_{c,in} A_{ch}}, \quad u_a = \zeta_a \frac{M_{H_2} I}{Y_{H_2,in}\rho_{a,in} A_{ch}} \tag{20}$$

where u_c and u_a are the inlet velocities and ζ_c and ζ_a the stoichiometry ratios for cathode and anode, respectively. M_{O_2} and M_{H_2} are the molar masses for oxygen and hydrogen. The mass fractions of oxygen and hydrogen at the inlets are represented by $Y_{O_2,in}$ and $Y_{H_2,in}$ and the densities for both gas mixtures, at the cathode and anode inlet boundaries are given by $\rho_{c,in}$ and $\rho_{a,in}$, respectively. At the channel outlet boundaries, Neumann boundary conditions (zero concentration gradient normal to the outlet face) are prescribed for the normal velocities, temperature and species equations. Pressure is prescribed at the outlet boundaries to match the desired operational pressure. The temperature at the surrounding walls of the channels is assumed to be constant.

2.4.2. Conservation equations in the gas diffusers

The gas transport in the GDs is restricted by the material's porosity, ε_{GD}, which is the fractional void volume. This changes the conservation equations in the following way:

$$\frac{\partial}{\partial x_j}\left(\rho \varepsilon_{GD} u_j\right) = 0 \tag{21}$$

$$u_j = -\frac{k_{p,GD}}{\mu}\frac{\partial p}{\partial x_j} \tag{22}$$

$$\frac{\partial}{\partial x_j}\left(\rho \varepsilon_{GD} u_j Y_m - D^{eff}_{m,GD}\rho \varepsilon_{GD}\frac{\partial Y_m}{\partial x_j}\right) = 0 \tag{23}$$

$$\frac{\partial}{\partial x_j}\left(\rho h_t \varepsilon_{GD} u_j - k^{eff}_{GD}(1-\varepsilon_{GD})\frac{\partial T}{\partial x_j} + \sum_m h_{t,m}\rho v_{m,j}\right) = u_j\frac{\partial P}{\partial x_j} + \tau_{ij}\frac{\partial u_i}{\partial x_j} \tag{24}$$

The mass, momentum, species and energy equations (Eqs. (21)–24) are reduced by ε_{GD}. The momentum equation has been replaced by Darcy's law, where $k_{p,GD}$ is the hydraulic permeability of the gas mixture in the GDs. The species binary diffusion coefficients in Eq. (23) are reduced by the Bruggeman correction [4]

$$D^{eff}_{mn} = D_{mn}\varepsilon^{\gamma_{GD}}_{GD} \tag{25}$$

where γ is the tortuosity of the medium.

Electric conduction through the GD fibers is modelled with Eq. (26). It relates the flux of current to the gradient of the electric potential ϕ_{e^-}. In this conduction process the charge is accelerated by an electric field and the intrinsic resistance of the conductive material

$$\frac{\partial}{\partial x_j}\left(-\kappa_{e^-,GD}\frac{\partial \phi_{e^-}}{\partial x_j}\right) = 0 \tag{26}$$

where $\kappa_{e^-,GD}$ is the electric conductivity of the GD.

It is assumed that the temperature of the CCs is uniform. Thereby a fixed temperature was defined at these boundaries. It is also assumed that the electric potential at this interface is fixed to a reference value, (see Section 2.5).

2.4.3. Conservation equations in the catalyst layers

In this region there are five transport processes: gas species transport through the pores, water transport through the hydrophilic electrolyte regions and void paths, heat conductivity through the solid matter, proton conductivity through the electrolyte fraction and electric conductivity through the carbon black particles.

All electrochemical reactions in a PEM fuel cell occur at these thin layers. A pseudo-homogeneous model of the CLs has been adopted from [6]. It has been assumed that all materials and properties of the CL have been homogeneously dispersed throughout its whole extent. Therefore, general values can be prescribed for the entire catalyst region.

The electric potential loss in the PEM is related to the fact that an electric field is necessary in order to maintain the motion of the protons through the membrane. This field is provided by the existence of a potential gradient across the cell, which is directed opposite from the outer field that gives the cell potential, and thus has to be subtracted. It can be shown that this loss obeys Ohm's law, [21]: hence, it can also be assumed that the transport of protons (Eq. (27)) is driven by a conduction process similar to the electric conductivity.

$$-\frac{\partial}{\partial x_j}\left(\sigma_{H^+}\varepsilon^{\gamma_{CL}}_{CL}\frac{\partial \phi_{H^+}}{\partial x_j}\right) = s_{H^+} \tag{27}$$

In Eq. (27)σ_{H^+} is the proton conductivity, which is not constant and s_{H^+} the source term for proton production. The proton conductivity is affected by the CL porosity, ε_{CL}. A similar relation to the Bruggerman correction is used to calculate the effective conductivity for protons in the electrolyte fraction of the CLs [2].

The source terms of the proton conservation equation (Eq. (27)), are defined as the rate of production of protonic charge per unit volume. This scalar is equal to the divergence of the current density, given by the current density divided by the thickness of the electrode on both, anode and cathode CLs, shown here in Eqs. (28)

$$s_{H^+,c} = -\frac{i_c}{t_{CL}}, \quad s_{H^+,a} = \frac{i_a}{t_{CL}} \tag{28}$$

where t_{CL} is the thickness of the catalyst layer. The electric conductivity in the CLs is modelled in the same way as in

the GDs

$$\frac{\partial}{\partial x_j}\left(-\kappa_{e^-,CL}\frac{\partial \phi_{e^-}}{\partial x_j}\right) = s_{e^-} \tag{29}$$

where $\kappa_{e^-,CL}$ refer to the CLs electric conductivity, which is assumed to be constant. Similarly, the rate of production of electric charge given in Eq. (29) at the anode and cathode CLs, follow those of the protons

$$s_{e^-,c} = \frac{i_c}{t_{CL}}, \quad s_{e^-,a} = \frac{i_a}{t_{CL}} \tag{30}$$

The conservation equations for mass, momentum, species and energy in the CLs are:

$$\frac{\partial}{\partial x_j}\left(\rho \varepsilon_{CL} u_j\right) = s_p \tag{31}$$

$$u_j = -\frac{k_{p,CL}}{\mu}\frac{\partial p}{\partial x_j} \tag{32}$$

$$\frac{\partial}{\partial x_j}\left(\rho \varepsilon_{CL} u_j Y_m + -D^{eff}_{m,CL}\rho \varepsilon_{CL}\frac{\partial Y_m}{\partial x_j}\right) = s_m \tag{33}$$

$$\frac{\partial}{\partial x_j}\left(\rho h_t \varepsilon_{CL} u_j - k^{eff}_{CL}(1-\varepsilon_{CL})\frac{\partial T}{\partial x_j} + \sum_m h_{t,m}\rho \nu_{m,j}\right) = u_j\frac{\partial P}{\partial x_j} + \tau_{ij}\frac{\partial u_i}{\partial x_j} + s_h - \sum_m H_m s_m \tag{34}$$

The binary diffusion coefficients for gases, $D^{eff}_{m,CL}$, in the CLs are calculated in a similar fashion as in the GD (Eq. (23)) using ε_{CL} instead. The source terms for the mass conservation equation in the cathode and anode catalyst layers (Eq. (31)) are given by Eqs. (35) and (36), respectively

$$s_{p,c} = \left(\frac{M_{H_2O}}{2F} - \frac{M_{O_2}}{4F}\right)\left(\frac{i_c}{t_{CL}}\right) + \dot{n}_{H_2O_{abs},c} \tag{35}$$

$$s_{p,a} = \left(-\frac{M_{H_2}}{2F}\right)\left(\frac{i_a}{t_{CL}}\right) + \dot{n}_{H_2O_{abs},a} \tag{36}$$

where M_{O_2}, M_{H_2} and M_{H_2O} are the molar masses of oxygen, hydrogen and water, respectively. The terms where the current density is divided by the thickness of the catalyst layer in Eqs. (35) and (36) refer to the rate of production of electric charge per unit volume.

The source terms for the oxygen and hydrogen conservation equation (Eq. (33)) in the CLs are given Eqs. (37) and (38), respectively

$$s_{O_2} = \left(-\frac{M_{O_2}}{4F}\right)\left(\frac{i_c}{t_{CL}}\right) \tag{37}$$

$$s_{H_2} = \left(-\frac{M_{H_2}}{2F}\right)\left(\frac{i_a}{t_{CL}}\right) \tag{38}$$

The main heat source in PEM fuel cells is given by the reduction reaction at the cathode CL. The heat sources of the CLs are given by Eqs. (39) and (40) for the cathode and anode, respectively.

$$s_{h,c} = \left[\frac{T(-\Delta \bar{s})}{4F} + \eta_{act,c}\right]\left(\frac{i_c}{t_{CL}}\right) + \frac{i_c^2}{\sigma^{eff}_{H^+}} \tag{39}$$

$$s_{h,a} = \frac{i_a^2}{\sigma^{eff}_{H^+}} \tag{40}$$

where $\Delta \bar{s}$ is the entropy change of the oxygen reduction reaction. The first term on the right-hand-side of Eq. (39) represents the energy loss due to entropy changes as well as irreversibilities with charge transfer [15]. The hydrogen oxidation reaction heat source is very small and has little effect in the cell performance [13].

2.4.4. Conservation equation for water in the electrolyte

The electrolyte in a PEM fuel cell is effectively a thin polymer membrane. It comprises the PEM and a fraction of the CLs (nafion content in the CLs). Its properties allow conduction of heat, water and protonic charge.

Water plays an important role in the overall cell performance because PEMs have to be hydrated in order to improve their protonic conductivity. Water distribution may hinder or enhance the fuel cell performance. On the one hand there is a risk of having excess water which will obstruct the transport of reactants to the catalyst sites due to the agglomeration of water in the porous medium. On the other hand de-humidification of the membrane may occur, reducing the protonic conductivity. In extreme cases of complete drying of the membrane, local burn-out of the electrolyte may take place and hydration strain becomes an adverse effect threatening the integrity of the material.

The conservation equation for water in the electrolyte is given as:

$$\frac{\partial}{\partial x_j}\left(f_{H_2O,j}\right) = 0 \tag{41}$$

where $f_{H_2O,j}$ is the diffusional flux of water inside the polymer. There are two driving forces that transport the water absorbed in the PEM, diffusion and electroosmotic drag.

The PEM absorbs water from the surrounding gases via the hydrophilic electrolyte fraction in the CLs. This happens when the equilibrium water content "(λ)" of this fraction is smaller than that of the surrounding gases. If on the contrary, the λ of the electrolyte fraction is higher than that of the surrounding gases then water will be given from the polymer to the surroundings. λ is defined as the ratio of the number of water molecules to the number of charged HSO_3 sites. Springer et al. [22] produced the following relationship for λ based on experiments performed on Nafion 117 membranes:

$$\lambda = 0.043 + 17.81a - 39.85a^2 + a^3 \quad a \leq 1 \tag{42}$$

$$\lambda = 14 + 1.4(a-1) \quad a > 1 \tag{43}$$

where the activity of water, a, is related to the partial pressure of water and the saturation pressure of water P_{sat}, according to:

$$a = \frac{X_{H_2O} P}{P_{sat}} \tag{44}$$

where X_{H_2O} is the molar fraction of water. The saturation pressure of water P_{sat} is given by expression (45) as reported by Springer et al. [22]

$$\log_{10} P_{sat} = -2.1794 + 0.02953T - 9.1837 \times 10^{-5} T^2 + 1.4454 \times 10^{-7} T^3 \tag{45}$$

where T is given in ° C and P_{sat} in atm. Note that when $\lambda > 1$ (i.e. Eq. (43)) the water vapour is in supersaturated conditions.

The single-phase assumption for water transport in this model implies that water can exist in supersaturation in the gas phase or if condensed, liquid water exists as finely dispersed droplets as in a mist flow and produces negligible effects on the gas phase transport. That is, the water activity calculated based on water partial pressure is allowed to be greater than unity.

The proton conductivity in the PEM is dependent upon water content λ and temperature. Springer et al. [22] measured the proton conductivity of Nafion for a range of water activities and temperatures with fully hydrated membranes. They found an activation energy value for these measurements. This activation energy was then assumed to apply for all values of λ. They obtained the following relation from a series of experiments σ_{H^+} as a function of λ:

$$\sigma_{H^+} = (0.0043119\lambda - 0.00326) \exp\left[1268\left(\frac{1}{303} - \frac{1}{T}\right)\right] \tag{46}$$

The properties reported by Springer et al. [22] are used in the baseline calculations. The conservation equation for proton transport in the PEM is then given by Eq. (47) as a pure electrical conduction process.

$$\frac{\partial}{\partial x_j}\left(-\sigma_{H^+} \frac{\partial \phi_{H^+}}{\partial x_j}\right) = 0 \tag{47}$$

The diffusion transport of the dissolved water in the membrane is related to its concentration gradient by an ordinary diffusion process, i.e. Fick's law of diffusion

$$f_{H_2O,j} = -\Gamma_{H_2O,m} \frac{\partial C_{H_2O}}{\partial x_j} \tag{48}$$

where $\Gamma_{H_2O,m}$ is the water diffusion coefficient in the electrolyte given in Eq. (49)[28]:

$$\Gamma_{H_2O,m} = 1 \times 10^{-10}\left(2.8628 \ln\left(\frac{\lambda}{1818}\right) - 1.63795\right) \tag{49}$$

The electroosmotic drag is associated with the protonic charge. It has been shown that the protonic charge in the membrane has a drag effect with water which is related to the polar structure of the water molecules [27]. This "adherence effect" makes the water molecules stick to the protons that are moving from one charged site to another, driving the water from the anode towards the cathode. The electroosmotic drag coefficient "n_d" is the number of water molecules carried per proton across the membrane as electric current is passed under conditions of no water concentration gradient. Because this mechanism is strongly influenced by the protonic charge, its transport can be related to the local current density via Eq. (50)

$$\dot{n}_{H_2O_{drag}} = n_d \left(\frac{i}{F}\right) \tag{50}$$

We assume that electroneutrality prevails inside the PEM. That is, the proton concentration in the polymer is assumed to be constant and equal to the concentration of the fixed sulfonic acid groups. Therefore the proton transport equation is conserved inside the PEM. Further the electroosmotic drag coefficient is assumed to be constant and equal to one [27]. In our model electroosmosis only occur where the local current density is variable, that is in the polymer fraction of the CLs, as indicated by Eq. (50). This does not mean that the electroosmotic drag has no effect on the water transport through the membrane. The electroosmotic drag term enters the water conservation equation as a boundary condition for the electrolyte fraction at the CLs. The total water flux should be equal to the electroosmotic drag and diffusive flux.

Water absorption and desorption take place on the polymer fraction (25%) inside the CLs. The rate of water absorption/desorption $\dot{n}_{H_2O_{abs}}$, is based on the difference between the equilibrium water content in the polymer fraction of the CLs, $C_{H_2O,m}$, and the water content of the gas mixture inside the pores of the CLs, $C_{H_2O,g}$. The water content of either can be calculated as

$$C_{H_2O} = \frac{\rho_{m,dry}}{M_{m,dry}} \lambda \tag{51}$$

where $\rho_{m,dry}$ and $M_{m,dry}$ are the density and molecular mass of a dry membrane.

Relation (52) states that when the water content of the polymer fraction is larger than that of the surrounding gases, then water should desorb from the membrane. It also indicates that if the water content of the surrounding gas is greater than that of the membrane, then water will be absorbed by the polymer.

$$\dot{n}_{H_2O_{abs}} = \psi\left(C_{H_2O,m} - C_{H_2O,g}\right) \tag{52}$$

where ψ is a proportionality constant set to 2.5. Higher or lower proportionality constants increase the concentration differences specially at high current densities. The value of ψ will mostly show its effect under time dependent calculation (STP or freezing conditions), Shimpalee et al. [18] reported values of ψ =1.5 for "start-up" calculation at 298 K and semi-dry membranes.

The absorbed and desorbed water plus the contribution of the electroosmotic drag at the anode (Eq. (54)) and cathode (Eq. (53)) CLs, are included into the water conservation equations via source terms

$$s_{H_2O,c} = \dot{n}_{H_2O_{drag},c} + \dot{n}_{H_2O_{abs},c} \tag{53}$$

$$s_{H_2O,a} = \left(\frac{M_{H_2O}}{2F}\right)\left(\frac{i_a}{t_{CL}}\right) + \dot{n}_{H_2O_{drag},a} + \dot{n}_{H_2O_{abs},a} \tag{54}$$

The first term on the right-hand-side of Eq. (54) accounts the "mass defect" due to the reactions. Note that the source terms on the species conservation equations do not inject or withdraw mass but instead adjust the concentration of species.

For heat transfer purposes, the membrane is considered a conducting solid slab. The conservation equation for energy in this region is given as

$$\frac{\partial}{\partial x_j}\left(k_{\text{mem}}^{\text{eff}}\frac{\partial T}{\partial x_j}\right) = s_{h,\text{mem}} \tag{55}$$

where $s_{h,\text{mem}}$ is an energy source term and $k_{\text{mem}}^{\text{eff}}$ is the effective heat conductivity of the membrane.

There is a heat source at the electrolyte given by Eq. (56), effectively due to ohmic heating

$$s_{h,m} = \frac{i^2}{\sigma_{\text{H}^+}^{\text{eff}}} \tag{56}$$

where i is the spatial electric current value.

2.5. Computational procedure

In most PEM fuel cell models the catalytic activity is a function of the concentration of the reactants. This dependence assumes a constant activation overpotential in the CLs. This method makes the solution process "easy" to handle; by assuming a constant activation overpotential, an average current density can be prescribed before the calculations. A specific current density in the cell can be scaled with concentration to match a desired average value.

Bang [2] reported a more detailed method regarding the kinetics in the catalyst layers. In this method the catalytic activity is a function of both concentrations and spatial variation of the overpotentials. The overpotentials are functions of the concentration of species and overpotentials at their spatial locations. This model assumes a variable overpotential in the CLs, simulating a variable kinetic activity in these regions. This way to address the cell overpotentials does not allow the user to predict a given current density before the calculations. Instead this comes as part of the solution.

The cell potential calculation is given as

$$E_{\text{cell}} = E_{\text{rev}} - \eta_{\text{act}} - \eta_{\text{ohm}} \tag{57}$$

The overpotentials in Eq. (57) are functions of their spatial location. To be able to calculate them at any given location in the MEA it was necessary to define voltage reference points. By convention the land area of the anode's GD was arbitrarily fixed to a zero potential boundary condition. This implies that the absolute potential in the anode's electrode is negative because the electric charge is being transferred from the anode reaction sites to the anode's GD/CC interface. The calculated cell potential is given at the cathode's GD/CC interface. The maximum potential is then given in the cathode's CL, as shown in Fig. 3. Within this context the ohmic overpotential η_{ohm} can be calculated by the protonic and electric overpotentials less their respective reference potential, as

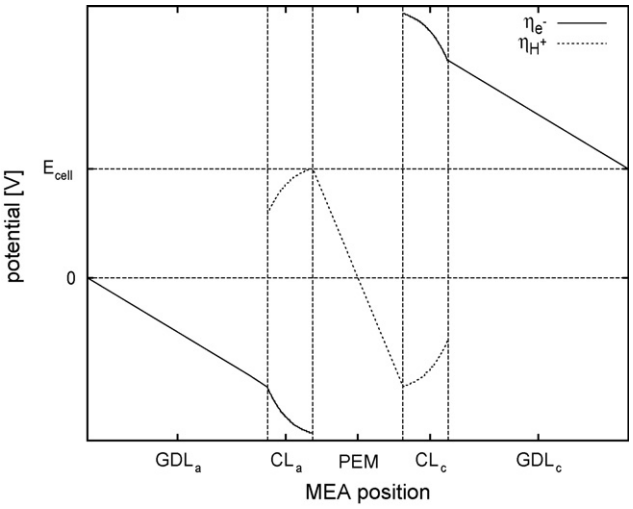

Fig. 3. Ohmic overpotential distributions across the membrane electrode assembly.

$$\eta_{\text{ohm}} = \left(|\eta_{\text{e}^-}| - |E_{\text{e}^-}^{\text{ref}}|\right) + \left(|\eta_{\text{H}^+}| - |E_{\text{H}^+}^{\text{ref}}|\right) \tag{58}$$

The protons generated in the anode CL travel towards the cathode CL. The potential losses of this process will be positive in the anode because of its positive source term, $s_{\text{H}^+,\text{a}}$, and will become negative as they travel towards the cathode, because of its negative source term $s_{\text{H}^+,\text{a}}$. However, the calculations deal with absolute values and this implies that there will be an "assumed" floating zero potential reference value lying at one point between the anode and cathode CLs. The position of this reference value becomes a function of the activity of the CLs. The overpotentials at each CL are updated on an iterative basis. As a result it is possible to determine a variable catalytic activity throughout the catalyst layers. By separating the losses at the CLs the activation overpotentials were calculated using

$$\eta_{\text{act,(a,c)}} = \eta_{\text{tot,(a,c)}} - |\eta_{\text{e}^-,\text{(a,c)}}| - |\eta_{\text{H}^+,\text{(a,c)}}| \tag{59}$$

2.6. Solution algorithm

The conservation equations given in this paper are not solved by the Star-CD solver in their differential form, but by the finite volume method, following a fairly well known CFD algorithm, known as SIMPLE [26].

Table 1
Sources and sink terms of the conservation equations

Equation	Anode CL	Electrolyte	Cathode CL
Mass	$s_{p,\text{a}}$	–	$s_{p,\text{c}}$
Energy	$s_{h,\text{a}}$	$s_{h,\text{mem}}$	$s_{h,\text{c}}$
Oxygen	–	–	s_{O_2}
Hydrogen	s_{H_2}	–	–
Water vapour	$s_{\text{H}_2\text{O,a}}$	–	$s_{\text{H}_2\text{O,c}}$
Potons	$s_{\text{H}^+,\text{a}}$	–	$s_{\text{H}^+,\text{c}}$
Electrons	s_{e^-}	–	s_{e^-}

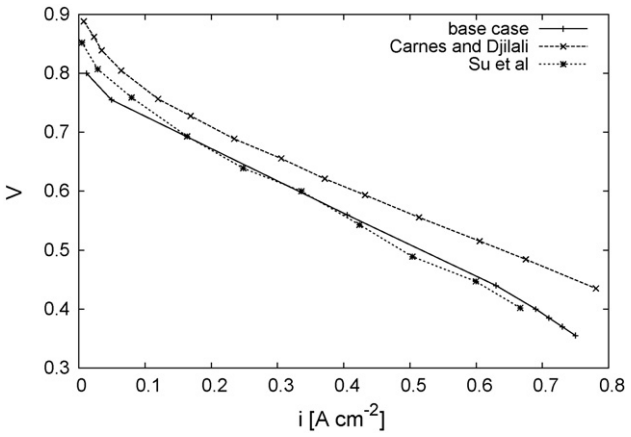

Fig. 4. Polarization curves of the "base case" and validation with a different numerical model and experimental data.

Table 2
Geometric and operational parameters used in the model's "base case"

Parameter	Value	Unit
Channel length	10	mm
Channel height	0.5	mm
Channel width	1	mm
GDL thickness	0.3	mm
GDL land area	10	mm^2
CL thickness	20	μm
PEM thickness	50	μm
Temperature	353	K
Pressure	1	atm
Hydrogen stoichiometry ratio	2	–
Hydrogen *R.H.* at inlet	100	%
Air stoichiometry ratio	2	–
Air *R.H.* at inlet	100	%

Table 3
Base case membrane electrode assembly parameters

Parameter	Symbol	Value	Unit
GDL porosity	ε_{GDL}	55	%
GDL tortuosity	γ_{GDL}	1.5	–
GDL heat conductivity	k^{eff}_{mem}	0.5	W $(mK)^{-1}$
GDL electric conductivity	$K_{e^-,GDL}$	825	S m^{-1}
CL porosity	ε_{CL}	13	%
CL tortuosity	γ_{CL}	2.5	–
CL heat conductivity	k^{eff}_{CL}	0.82	W $(mK)^{-1}$
CL electric conductivity	$K_{e^-,CL}$	250	S m^{-1}
Pt mass loading per unit area of CL	ml_{Pt}	0.6	mg cm^{-2}
Mass of Pt supported on carbon black	mp_{Pt}	20	%
Nafion volume fraction in CL	–	25	%
PEM heat conductivity	k^{eff}_{CL}	0.64	W $(mK)^{-1}$
Anode's transfer coefficient	α_a	0.5	–
Cathode's transfer coefficient	α_c	0.5	–
Anode's exchange current density	$i_{0,a}$	8.0×10^3	A m^{-2}
Cathode's exchange current density	$i_{0,c}$	4.0×10^{-8}	A m^{-2}

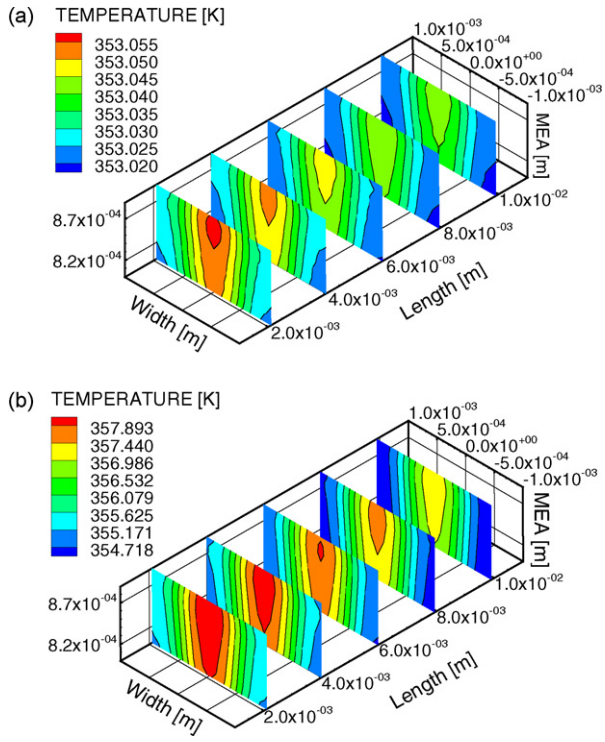

Fig. 5. Temperature distribution across the MEA at different cell potentials. (a) Temperature distribution across the MEA at $E_{cell} \approx 0.8$ V and $i \approx 0.01$ A cm^{-2} (T1jps.eps). (b) Temperature distribution across the MEA at $E_{cell} \approx 0.35$ V and $i \approx 0.75$ A cm^{-2}.

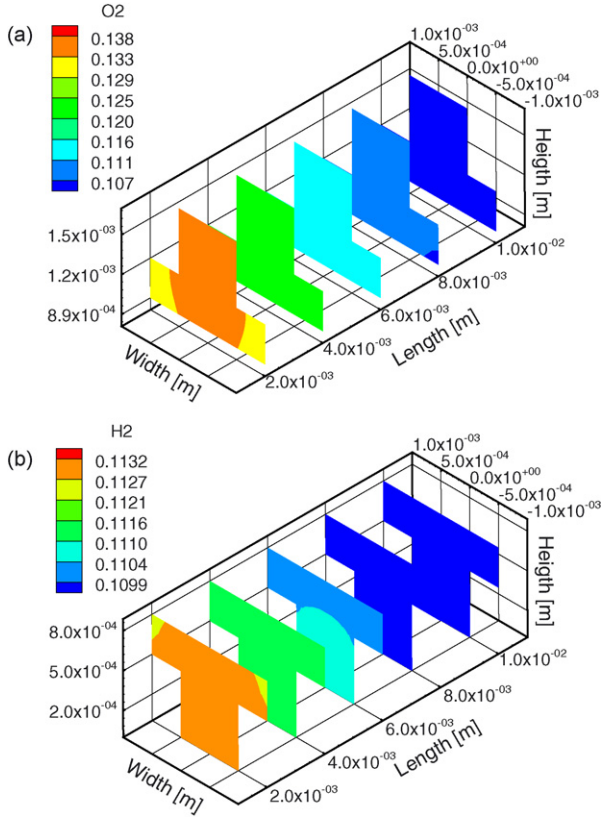

Fig. 6. Oxygen and hydrogen mass fractions at $\iota = 0.012$ A $cm^{-2}$and $E_{cell} =$ 0.8 V. (a)Oxygen mass fraction in the cathode at 0.012 A $cm^{-2}$and 0.8 V. (b) Hydrogen mass fraction in the anode at 0.012 A cm^{-2} and 0.8 V.

The user-defined code forms part of this algorithm. It begins with a prescribed total overpotential at the cathode CL then the current density is first calculated and stored for the cathode side. Following this, the anode's activation overpotential is tuned in order to match the cathode's total current. The code loops through the anode catalyst layer a certain number of times per iteration in order to approximate the two total currents. If both anode and cathode currents still do not match after this number of loops the algorithm continues and iterates again. The iterative process changes several variables such as temperature, density, diffusion coefficients, scalar concentrations, proton conductivity, overpotentials, etc. With the calculated total current, the cell potential can be calculated with an updated value of the overpotentials. The procedure continues until the anode and cathode total currents match (Table 1).

The computations were preformed on a machine with a 1.4 GHz processor and 512 MB of memory. To obtain a single solution, about four to eight thousand iterations were required and took from 4 to 10 h of CPU time (the latter corresponds to the high and very low current densities). The flowchart diagram of the algorithm is shown in Fig. 1.

3. Results and discussions

The model was tested under a range of operational conditions. Fig. 4 shows a good agreement between the "base case" results, experimental tests performed by Su et al. [24] and another PEM fuel cell model presented by Carnes and Djilali [7].

3.1. Base case model

The base case model presented in this section is the foundation of the analyses performed in this paper. It represents the closest attempt by the authors to resemble a functional PEM fuel cell. The geometric parameters and operation conditions of the base case model are listed in Table 2.

Table 3.

The temperature field measured in the PEM is shown in Fig. 5 for two different potentials. These figures show how the temperature can increase by up to 5 ° C at the given potentials. In a PEM fuel cell the major heat source comes from the entropy change of the oxygen reduction reaction. That is why it is always the top part (cathode) of Fig. 5 is slightly warmer than the bottom (anode). The secondary source of heat in this type of cells comes from the ohmic resistance of the PEM to ionic conductivity, this also contributes to the heating of the cell.

Figs. 6 and 7 show contour planes used to illustrate the concentration of the reactants. Each plane includes the channel and GD for both anode and cathode sides of the cell. The base case model oxygen and hydrogen concentrations are shown in these figures for two different potentials. The figures show how, at

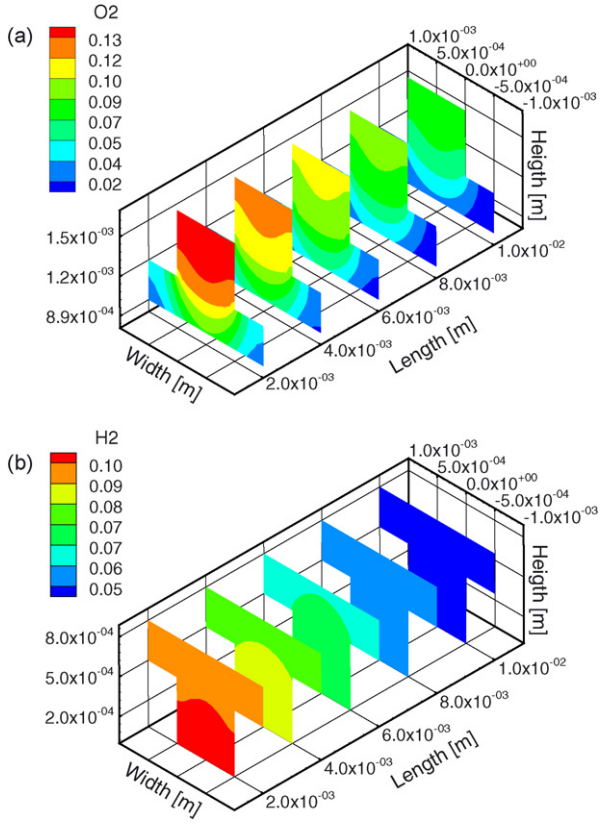

Fig. 7. Oxygen and hydrogen mass fractions at $\iota = 0.77\,\mathrm{A\,cm^{-2}}$ and $E_{\mathrm{cell}} = 0.37\,\mathrm{V}$. (a) Oxygen mass fraction in the cathode at $0.77\,\mathrm{A\,cm^{-2}}$ and 0.37 V. (b) Hydrogen mass fraction in the anode at $0.77\,\mathrm{A\,cm^{-2}}$ and 0.37 V.

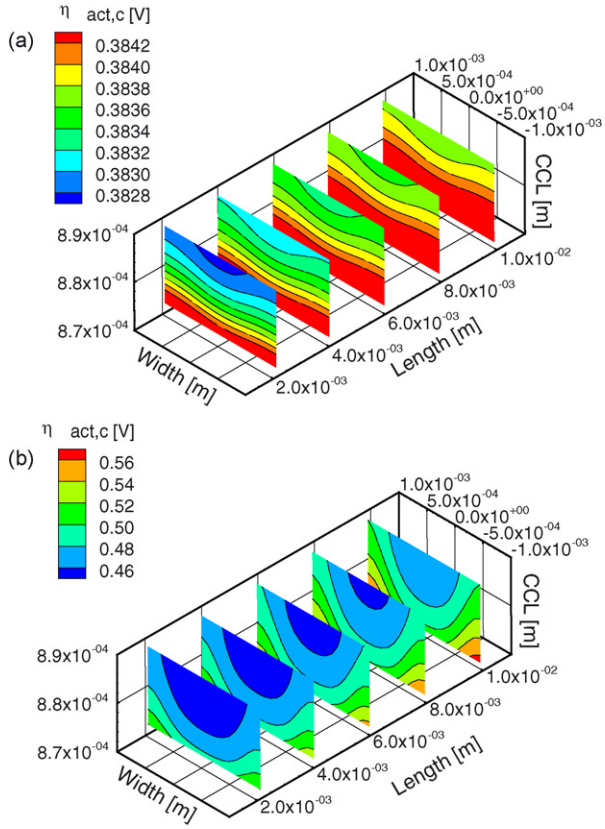

Fig. 8. Activation overpotential distributions in the cathode's catalyst layer at different cell potentials. (a) Activation overpotential distribution in the cathode's catalyst layer at $0.01\,\mathrm{A\,cm^{-2}}$ and 0.8 V. (b) Activation overpotential distribution in the cathode's catalyst layer at $0.77\,\mathrm{A\,cm^{-2}}$ and 0.37 V.

high current densities, the reactants are consumed faster than at lower current densities. It is clear that at these current densities the most affected species is the oxygen. In fact, at these power densities part of the model's MEA is depleted of oxygen specifically in the regions under the current collectors, as shown in Fig. 7(a). This is partly due to a limited oxygen diffusivity and also due to the difficulty in removing the water produced by the oxygen reduction reaction.

On the other hand, it can be seen that on the anode side of the cell, the hydrogen concentration experiences little change. Hydrogen has a higher diffusivity than oxygen and this allows a better transport even at high current densities and low porosities. In the model presented in this paper hydrogen posed no depletion threat. In addition, the anode side of the cell rarely experiences flooding, therefore its porous medium is almost never blocked.

One important feature of the model presented in this paper is the way the activation overpotential is calculated. As explained earlier in Section 2.5, the overpotentials of the cell are calculated as a function of the species concentration.

The CCL alone, is represented in Figs. 8 and 9 and because it is only 20 μm thick it has been scaled by several factors in the *Y* direction. These figures illustrate the activation overpotential and the local current density distribution in this region. Fig. 8(a) shows how at a low current density the activation overpotential is fairly uniform throughout the CCL. However, as the current density increases the concentration of the reactants decreases and this has a negative effect in the activation overpotential distribution, as shown in Fig. 8(b). Here the activation overpotential is not uniform, the maximum values of the activation overpotential move towards the lower region of the CCL (close to the CCL/PEM interface) under the current collector ribs. The minimum values always stay on top of the CCL right below the cathode channel.

These activation overpotential distributions have other effects in the cell. The Butler-Volmer Eqs. (3) and (4) described the relation between the activation overpotential and the local current density. Fig. 9 shows how the local current density varies throughout the CCL. At a low potential the local current density is evenly distributed, as shown in Fig. 9(a). At high power densities however, the current distribution is totally uneven (Fig. 9(b)). The CCL becomes a region of contrasts. Near the CCL/PEM the current is 10 times bigger than its immediate upper region. This means that only the very bottom layer of the CCL is powering the cell. At high current densities the overpotentials near the CCL/PEM interface are so big that almost 90% of the whole power density generated in the cathode is produced at this very thin layer.

Due to the importance of oxygen in the overall cell performance its concentration in the CCL is shown in Fig. 10. Note how under the current collector ribs the concentration of oxygen is reduced gradually as the current density increases. Once again, the same tendency of the current density and activation over-

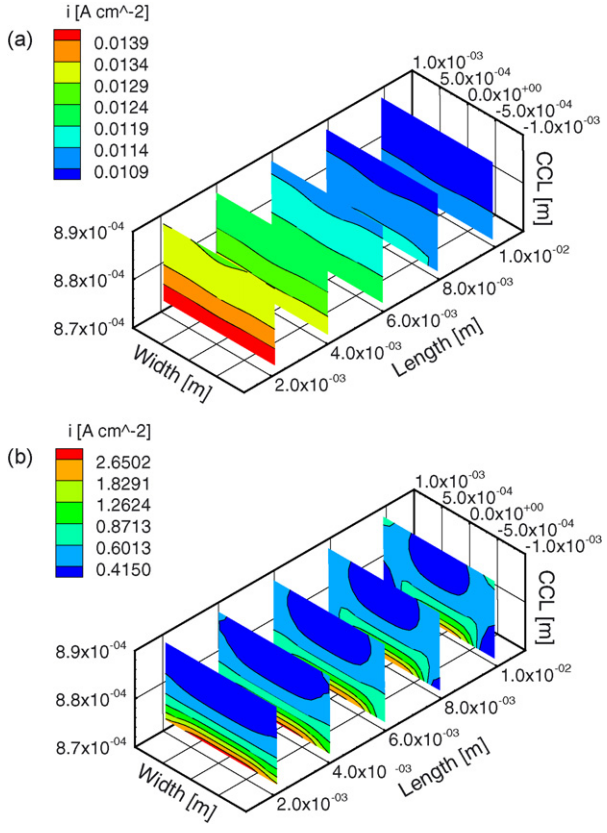

Fig. 9. Current density distributions in the cathode's catalyst layer at different cell potentials. (a) Current density distribution in the cathode's catalyst layer at 0.01 A cm^{-2} and 0.8 V. (b) Current density distribution in the cathode's catalyst layer at 0.77 A cm^{-2} and 0.37 V.

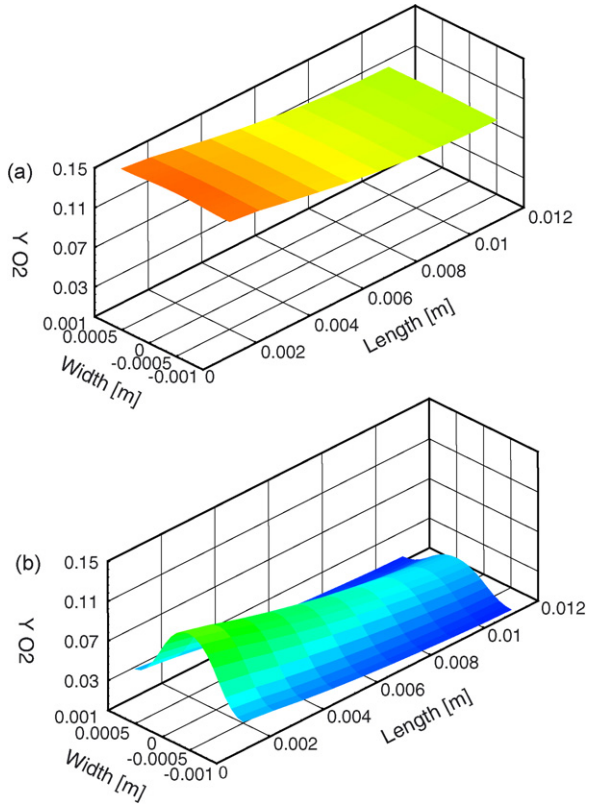

Fig. 10. Oxygen concentrations in the cathode's catalyst layer at different cell potentials. (a) Oxygen concentration in the cathode's catalyst layer at 0.01 A cm^{-2} and 0.8 V. (b) Oxygen concentration in the cathode's catalyst layer at 0.77 A cm^{-2} and 0.37 V.

potential is reflected in these figures. At low current densities the availability of oxygen is good enough to fulfill the reactant requirements (Fig. 10(a)). However, at high current densities the oxygen diffusivity becomes a problem, as it cannot provide the rate needed to drive the reaction further. At this current densities, starvation regions are clearly present under the current collector ribs, Fig. 10(b).

As explained earlier in Section 2.5, the activation overpotential is a sum of other overpotentials of a different nature. The following figures show the distribution of these losses in the cell. Ohmic overpotentials: ionic and electronic, are always present and play active roles in the calculation of the activation overpotential. Due to the intrinsic electric resistance of the materials in the cell the losses of these two overpotentials become greater as the current density increases.

Fig. 11 shows the protonic overpotential distribution at two different current densities. The loss is the most severe out of the two ohmic overpotentials. In this model it is a function of the membrane water content and temperature. The proton and water distribution in the membrane are related by the electroosmotic drag effect. A special procedure to model this relationship was presented in Section 2.5. This method requires a reference potential (0 V) located in between the two CLs. However, this reference potential has a variable position; Fig. 11(a) shows how

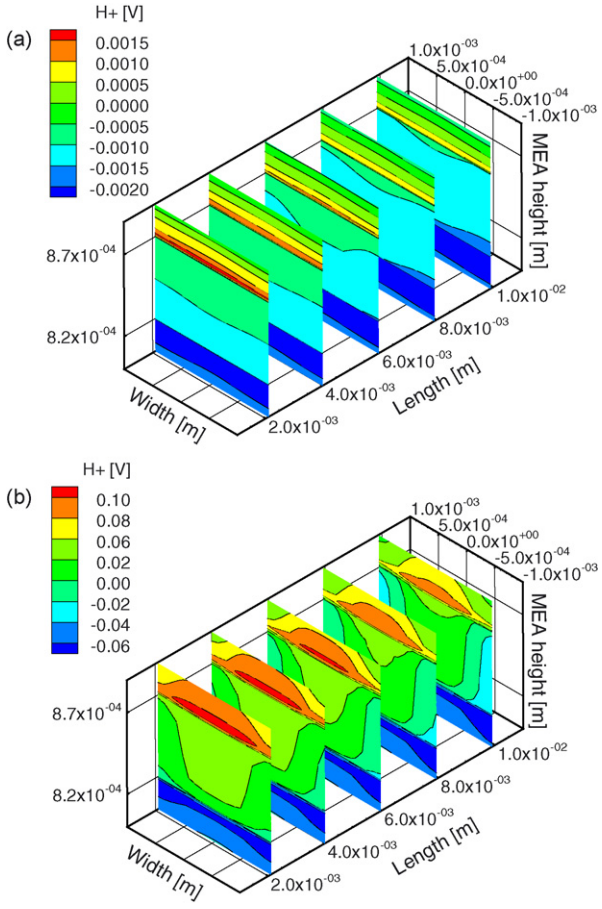

Fig. 11. Protonic overpotential distributions at different cell potentials. (a) Protonic overpotential distribution at 0.01 A cm^{-2}and 0.8 V. (b) Protonic overpotential distribution at $\eta_{H^+,c}$ at 0.77 A cm^{-2} and 0.37 V.

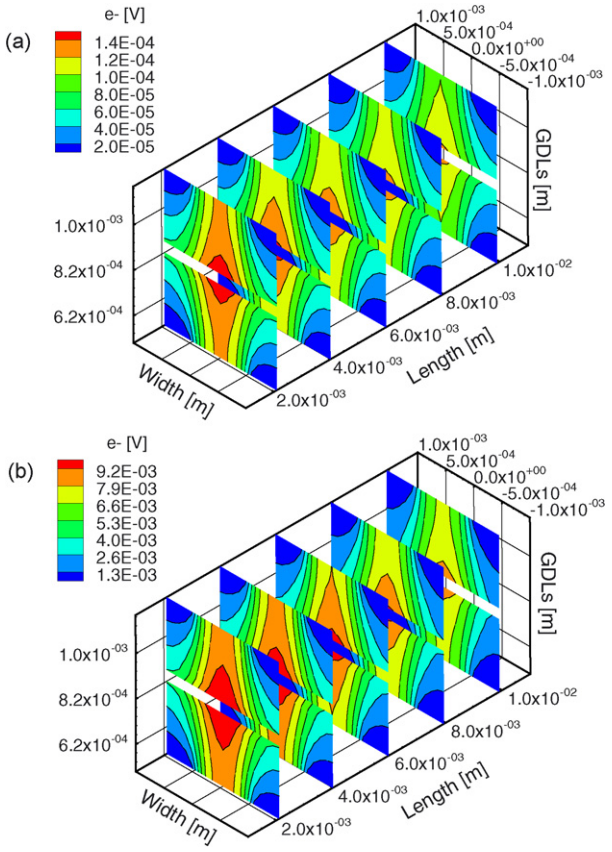

Fig. 12. Electric overpotential distributions at different cell potentials. (a) Electric overpotential distribution at 0.77 A cm^{-2}and 0.38 V. (b) Electric overpotential distribution at 0.77 A cm^{-2}and 0.37 V.

at a low current is hard to distinguish were the reference value lies. At this power density the ohmic losses are small and the biggest losses are located at the anode CL. Fig. 11(b) shows how the reference value lies clearly in between the two CLs adopting a curved shape under the current collector ribs. The biggest losses at this power density are clearly located close to the cathode CL.

Fig. 12 shows the distribution of the electric overpotentials in the GDs. Similar to the protonic losses, the electric overpotential also uses reference voltages. In this case these reference potentials are stationary. These are set as boundary conditions at the interfaces between the GDs and the current collector ribs. This condition is reflected in the shape of the contours of Fig. 12. The electric overpotential is highest at the region under the channels and closer to the inlet boundaries. Once again, it can be seen that the higher the current density the higher the overpotential.

The protonic and electric overpotential are two conduction processes restricted by the resistance of the materials. The protonic diffusion coefficient is calculated as a function of temperature and water content of the membrane (see Section 2.4.4).

4. Conclusions

A comprehensive three-dimensional model of a PEM fuel cell has been developed. The model accounts for all major transport phenomena in the cell with a single-phase assumption. The

transport equations and boundary conditions of each of the cell's regions were introduced along with some special boundary conditions such as the inlet velocity and the CL and PEM interfaces. A thorough explanation of the processes occurring inside the electrolyte was given in Section 2.4.4. It began with the equilibrium water content and continued with water diffusion and electroosmotic drag and their impact upon proton and water conductivity.

We produced a good agreement of the model's performance with some other experimental and numerical models. Some illustrations of the model operating at different conditions showed how the reactants distribute throughout the cell. The temperature distribution in the PEM at different cell potentials showed how the temperature gradient could hinder the material integrity of the membrane. It was shown how the current density distributes across the cathode CL (Fig. 9). To our knowledge these current density distributions have long been measured in experiments but never published in a computational model. Similarly the distribution of the overpotentials were shown in the gas diffusers, catalyst layers and in the electrolyte.

Acknowledgements

The work presented in this paper has been funded by the "Instituto Mexicano del Transporte". I would like to extend my gratitude to Dr. M. Bang and the thermofluid group at the Institute of Energy and Technology at Aalborg University for their contribution to the development of the model.

References

[1] C.M. Baca, Computational model of a PEM fuel cell, Ph.D. Thesis, Imperial College London, London, UK, 2007.
[2] M. Bang, Modeling of diffusive convective and electrochemical processes in PEM fuel cells, Ph.D. Thesis, Aalborg University, Aalborg, Denmark, 2004.
[3] J.J. Bard, L.R. Faulkner, Electrochemical Methods, Wiley, 1980.
[4] J. Bear, M. Buchlin, Modelling and Applications of Transport Phenomena in Porous Media, Springer, 1991.
[5] D.M. Bernardi, M.W. Verbrugge, J. Electrochem. Soc. 139 (1992) 2477.
[6] D. Bevers, M. Wohr, K. Yasuda, K. Oguro, J. Appl. Electrochem. 27 (1997) 1254.
[7] B. Carnes, N. Djilali, J. Power Sources 144 (2005) 83.
[8] E.L. Cussler, Diffusion, Mass Transfer in Fluid Systems, Cambridge University Press, 1997.
[9] S. Dutta, S. Shimpalee, J.W. Van Zee, Three-dimensional numerical simulation of straight channel PEM fuel cells, J. Power Sources 86 (2000) 181.
[10] S. Dutta, S. Shimpalee, J.W. Van Zee, Int. J. Heat Mass Transfer 44 (2001) 2029.
[11] T.F. Fuller, J. Newman, J. Electrochem. Soc. 140 (1993) 1218.
[12] V. Gurau, H. Liu, S. Kakac, AIChE J. 44 (1993) 2410.
[13] J. Hyunchul, M. Hua, W. Chao-Yang, Int. J. Heat Mass Transfer 48 (2005) 1303.
[14] A.A. Kulikovsky, J. Electrochem. Soc. 150 (2003) 1432.
[15] M.J. Lampimen, M. Fomino, J. Electrochem. Soc. 140 (1993) 3537.
[16] W.K. Lee, J.W. Van Zee, S. Shimpalee, S. Dutta, editors. Effect of humidity on PEM fuel cell performance. Part I. Experiments, Presented at the International Mechanical Engineering Congress and Exposition, 1999.
[17] W.K. Lee, J.W. Van Zee, S. Shimpalee, S. Dutta, editors. Effect of humidity on PEM fuel cell performance. Part II. Numerical simulations, Presented at the International Mechanical Engineering Congress and Exposition, 1999.
[18] W. Lee, S. Shimpalee, J.W. Van Zee, J. Electrochem. Soc. 150 (2003) A341.
[19] S. Mathur, P.K. Tondon, S.C. Saxena, Mol. Phys. 12 (1967) 569.
[20] A.F. Mills, Heat and Mass Transfer, Irwin, 1995.
[21] K.B. Oldham, J.C. Myland, Fundamentals of Electrochemical Science, Academic Press, 1994.
[22] T.E. Springer, T.A. Zawodzinski, S. Gottesfeld, J. Electrochem. Soc. 138 (1991) 2334.
[23] P.C. Sui, N. Djilali, J. Fuel Cell Sci. Technol. 2 (2005) 1.
[24] A. Su, F.-B. Weng, C.-Y. Hsu, Y.-M. Chen, Int. J. Hydrogen Energy 31 (2006) 1031.
[25] E.A. Ticianelli, C.R. Derouin, A. Redondo, S. Srinivasan, J. Electrochem. Soc. 135 (1988) 2209.
[26] H.K. Versteeg, W. Malalasekera, An Introduction to Computational Fluid Dynamics, Prentice Hall, 1995.
[27] T.A. Zawoszinski, J. Davey, J. Valerio, S. Gottesfeld, Electrochim. Acta 40 (1995) 297.
[28] T.A. Zawoszinski, T.E. Springer, J. Davey, J. Valerio, S. Gottesfeld, editors. Proceedings of the Symposium on Modelling of Batteries and Fuel Cells, The Electrochemical Society, Battery Division, 1991.